Biochimica et Biophysica Acta 1860 (2016) 434–444

Contents lists available at ScienceDirect

Biochimica et Biophysica Acta

journal homepage: www.elsevier.com/locate/bbagen

Protein conformational perturbations in hereditary amyloidosis: Differential impact of single point mutations in ApoAI amyloidogenic variants

Rita Del Giudice [a], Angela Arciello [a,e], Francesco Itri [a], Antonello Merlino [a,b], Maria Monti [a,e], Martina Buonanno [b,c], Amanda Penco [d], Diana Canetti [a,e], Ganna Petruk [a], Simona Maria Monti [b], Annalisa Relini [d,e], Piero Pucci [a,e], Renata Piccoli [a,e], Daria Maria Monti [a,e,*]

[a] Department of Chemical Sciences, University of Naples Federico II, 80126 Naples, Italy
[b] Institute of Biostructures and Bioimaging-CNR, Via Mezzocannone 16, 80134 Naples, Italy
[c] Dipartimento di Scienze e Tecnologie Ambientali, Biologiche e Farmaceutiche, Seconda Università di Napoli, Caserta, Italy
[d] Department of Physics, University of Genoa, Genoa, Italy
[e] Istituto Nazionale di Biostrutture e Biosistemi (INBB), Rome, Italy

ARTICLE INFO

Article history:
Received 17 July 2015
Received in revised form 15 October 2015
Accepted 23 October 2015
Available online 26 October 2015

Keywords:
Apolipoprotein A I
Protein stability
Amyloidosis
Conformational diseases

ABSTRACT

Amyloidoses are devastating diseases characterized by accumulation of misfolded proteins which aggregate in fibrils. Specific gene mutations in Apolipoprotein A I (ApoAI) are associated with systemic amyloidoses. Little is known on the effect of mutations on ApoAI structure and amyloid properties. Here we performed a physico-chemical characterization of L75P- and L174S-amyloidogenic ApoAI (AApoAI) variants to shed light on the effects of two single point mutations on protein stability, proteolytic susceptibility and aggregation propensity. Both variants are destabilized in their N-terminal region and generate fibrils with different morphological features. L75P-AApoAI is significantly altered in its conformation and compactness, whereas a more flexible and pronounced aggregation-competent state is associated to L174S-AApoAI. These observations point out how single point mutations in ApoAI gene evocate differences in the physico-chemical and conformational behavior of the corresponding protein variants, with the common feature of diverting ApoAI from its natural role towards a pathogenic pathway.

1. Background

Amyloidoses are characterized by protein aggregation in insoluble fibrils and their deposition in tissues and organs, with consequent alteration of their functionality. To date, almost 30 amyloidogenic proteins have been identified [1]; although these proteins do not show any sequence or structure homology, they have the ability to give rise to amyloid fibrils characterized by a highly ordered and rigid structure [2–5].

Apolipoprotein A I (ApoAI) is the main component of high density lipoproteins (HDL) and is mostly involved in the removal of cholesterol from peripheral tissues and its transfer, via the plasma, to the liver, where it is either recycled back to plasma as a component of newly formed lipoproteins, or excreted from the body via bile [6]. Due to ApoAI conformational plasticity, in its lipid-free or lipid-poor form, this protein is able to bind to phospholipids and to unesterified cholesterol to give rise to nascent HDL [7].

Some of the mutations in ApoAI gene are associated with hereditary systemic amyloidoses, characterized by extracellular fibrillar deposits in specific tissues, mainly heart, liver, kidneys and testes [8–10]. It has been reported that in the HDLs of heterozygous patients, in which both the wild-type protein and an amyloidogenic variant (L75P-AApoAI, L174S-AApoAI or L64P-AApoAI) are present, the wild-type protein is more abundant than the variant [11–13]. This finding is in line with our recent observation that in stably transfected human hepatic cells over-expressing L75P-AApoAI the secretion of the amyloidogenic variant is down-regulated [14], which in turn is in line with the observation of Marchesi and coworkers, who reported a decreased secretion efficiency of L75P- and L174S-AApoAI variants in transiently transfected COS cells [15]. Moreover, it has been hypothesized that AApoAI variants have a lower affinity for HDLs when compared to the wild-type protein; this would shift the ApoAI distribution from HDL-bound to lipid-poor/free state, which is relatively unstable and susceptible to proteolysis. The

Abbreviations: ANS, 8-anilino-1-naphthalensulfonic acid; ApoAI, apolipoprotein A I; AApoAI, amyloidogenic apolipoprotein A I; CD, circular dichroism; DLS, dynamic light scattering; GdnHCl, guanidine hydrochloride; HDL, high-density lipoproteins; MD, molecular dynamics; ThT, thioflavin T; TM-AFM, tapping mode atomic force microscopy; LC-MS, liquid chromatography-mass spectrometry.

* Corresponding author at: Department of Chemical Sciences, University of Naples Federico II, 80126 Naples, Italy.
E-mail address: mdmonti@unina.it (D.M. Monti).

http://dx.doi.org/10.1016/j.bbagen.2015.10.019
0304-4165/

resolution at 2.2 Å of the crystal structure of lipid-free Δ(185–243)-ApoAI revealed that ApoAI associates in domain swapped dimers held together by two four-helix bundles each constituted by the N-terminus of one subunit and the C-terminus of its partner. Interestingly, all the 19 amyloidogenic mutations so far identified cluster in two regions: the amino-terminus (residues 1–100) and within residues 173–178 [16], which, in the dimeric structure, define a 3D hot-spot mutation site [17]. To date, only few full-length AApoAI variants, out of 19 identified so far, have been investigated, which show significant peculiarities on the conformational transitions [18–21]. Recently, a model has been proposed, prompting that AApoAI mutations perturb one of the 4 predicted hot spots of the protein (14–22, 53–58, 69–72 and 227–232), with consequent full-length protein aggregation via the N-terminal region. This event would be followed by proteolytic cleavage at the exposed loop (83–100) and release of the N-terminal fibrillogenic polypeptide [21], which has been found to be the main protein constituent of ex-vivo fibrils [8]. It has been hypothesized that perturbation in the hot spots is one of the prerequisite for AApoAI misfolding, even though other factors may influence this process [21]. Here we analyzed the effects of two point mutations, L75P and L174S, on AApoAI conformational stability, being the former an "inside" mutation, i.e. located within the N-terminal fibrillogenic polypeptide, and the latter an "outside" mutation. Leu 75 is located in the middle of the short helix 70–76 that contributes to define the relative helical orientation in the four-segment bundle, whereas Leu 174 is located in the "bottom" of the hydrophobic cluster [22]. The variant with leucine to proline substitution at position 75 (L75P-AApoAI) is associated with a hereditary systemic amyloidosis characterized by preferential accumulation of fibrils in the kidneys and liver [11]. Instead, in the case of leucine to serine substitution at position 174 (L174S-AApoAI), a predominant accumulation of fibrils in the heart, skin, testes and larynx was observed [12]. The molecular basis of this differential localization of amyloid fibrils is still unknown.

We report structural stability, proteolytic susceptibility and aggregation propensity of full-length recombinant, lipid-free, human AApoAI harboring L75P or L174S mutation, to reveal the effects of a single point mutation on AApoAI structure and amyloidogenic potential.

This study is aimed to add knowledge to the largely unknown field of systemic amyloidoses. Starting from the general hypothesis suggesting that single point mutations, occurring in the 3D hot spot mutation site, direct the protein towards an amyloidogenic pathway, our study is aimed at revealing common and different impacts of mutations on protein stability.

2. Methods

2.1. Production of recombinant proteins

A bacterial expression system consisting of ApoAI expressing pET20 plasmid in *Escherichia coli* strain BL21(DE3) pLysS (Invitrogen) was used to prepare AApoAI proteins, as previously described [18]. Primer-directed PCR mutagenesis was used to introduce the L75P and L174S mutations. The mutation was verified by dideoxy automated fluorescent sequencing. Human ApoAI proteins were purified from bacterial cell lysate by immobilized metal affinity chromatography (HiTrap columns, GE Healthcare, Waukesha, WI) under denaturing conditions (4 M urea). Following binding, an extensive wash with 500 mM NaCl and 4 M urea in sodium phosphate buffer, 20 mM, pH 7.4 (wash buffer) was performed and bound proteins were then eluted with 500 mM imidazole in wash buffer. Proteins were dialyzed versus refolding buffer (50 mM Tris–HCl, pH 7.4), concentrated with 30 kDa molecular weight cut-off Amicon Ultra centrifugal filter devices (Millipore), and stored at −20 °C.

Purity and identity of the wild-type and variants were confirmed by LC–MS analyses, as reported below. Chromatographic traces recorded for each protein preparation, showed a single sharp peak, corresponding to the recombinant protein and the measured molecular masses were in agreement with the theoretical ones, according to the amino acid sequences of his-tagged expressed constructs (wild-type ApoAI: measured molecular mass: 29,799.6 ± 1.1 Da, theoretical molecular mass: 29,798.5 Da; L75P-AApoAI: measured molecular mass: 29,783.0 ± 1.8 Da, theoretical molecular mass: 29,782.5 Da; L174S-AApoAI: measured molecular mass: 29,772.8 ± 1.5 Da, theoretical molecular mass: 29,772.4 Da). For all the experiments His-tag containing proteins were used, as in preliminary conformational analyses (data not shown) we did not observe any significant difference comparing the His-tag containing wild-type protein to the protein after His-tag removal, or to commercial ApoAI (Sigma-Aldrich).

2.2. CD spectroscopy

Circular dichroism (CD) measurements were performed on a Jasco J815 spectropolarimeter (Jasco, Essex, UK), equipped with a temperature control system, using a 1-mm quartz cell in the far-UV range 194–260 nm (50 nm/min scan speed). Each spectrum was the average of three scans with the background of the buffer solution subtracted. Measurements were performed at 25 °C at a protein concentration of 0.15 mg/mL in 50 mM Tris HCl pH 7.4. Raw spectra were corrected for buffer contribution and converted to mean residue ellipticity, θ (mdeg cm^2 $dmol^{-1}$). Estimation of the secondary structure was carried out according to the Variable Selection Method (CDSSTR) using DICHROWEB [23].

2.3. Intrinsic fluorescence analysis

Emission fluorescence spectra were recorded in the range 300–450 nm, following excitation at 280 (tyrosine/tryptophan) or 295 nm (tryptophan). Measurements were carried out at 25 °C in a 10 mm cell by using a Perkin-Elmer LS50 spectrofluorimeter. Emission spectra were acquired at a scanning speed of 300 nm/min, with 10 and 5 slit widths for excitation and emission, respectively. Proteins (3 μM) were analyzed in 50 mM Tris HCl at pH 7.4.

2.4. Dye-binding assays

2.4.1. ThT binding assay

Proteins (0.3 mg/mL) were incubated at 25 °C in 50 mM Tris HCl at pH 7.4 in the presence of 10 μM thioflavin T (ThT). ThT fluouorescence emission spectra were acquired in the range 470–490 nm at 1 h intervals with scan speed of 300 nm/min, upon excitation at 450 nm. Excitation and emission slits were set at 5 and 10 nm, respectively. Fluorescence intensity values at 482 nm were plotted as a function of time. The determination of apparent $t_{1/2}$ values was obtained by non-linear regression fit of the data according to a double Boltzmann equation. The reported values represent the means from three independent experiments.

2.4.2. 1-Anilinonaphthalene-8-sulfonic acid (ANS) binding assay

Emission fluorescence spectra of recombinant proteins (3 μM) were acquired in the presence of the dye ANS (350 μM). Analyses were performed in 50 mM Tris HCl at pH 7.4, at 25 °C. Emission fluorescence spectra were recorded in the range 400–600 nm, following excitation at 380 nm. Excitation and emission slits were set at 5 and 10 nm, respectively.

2.5. Protein stability to denaturing agents

2.5.1. Chemical denaturation

Equilibrium denaturation was carried out on samples using guanidine (GdnHCl) and urea. Proteins were incubated for 24 h at 4 °C at 0.05 mg/mL prior to addition of denaturant. Incubated proteins were combined with denaturant, diluted from 8 M stock solutions. Samples were stored at 4 °C for 24 h prior to data collection. Changes in tryptophan fluorescence were recorded. The unfolding transition was

monitored by recording the wavelength at maximum fluorescence intensity (λ_{max}). The λ_{max} of triplicate dilutions of each sample was averaged and plotted against the denaturant concentration. Experimental points, describing sigmoidal curves, were fitted using the Boltzmann equation and $D_{1/2}$ (the concentration of denaturant at which the protein is half folded) was calculated. Assuming a two-state model (folded and unfolded), the free energy of denaturation was calculated as described by Petrlova et al. [18] by using the equation: $\Delta G_D^\circ = -RTlnK_D$. ΔG_D° and m values were obtained by plotting ΔG_D versus denaturant concentration to give the linear equation [24] $\Delta G_D = \Delta G_D^\circ - m[denaturant]$, where ΔG_D° is the free energy of protein folding in water (0 M denaturant), and m the cooperativity of denaturation.

2.5.2. Thermal denaturation

Temperature-induced denaturation of proteins (0.05 mg/mL) was performed as a function of increasing temperature (20–100 °C). Protein samples were incubated at the desired temperature for 15 min before taking the measurements. Denaturation of proteins was performed by recording changes in tryptophan fluorescence.

2.6. Homology modeling and molecular dynamics simulations

The starting structure of wild-type ApoAI for molecular dynamics simulation was taken from the protein data bank (PDB) file 3R2P [17]. The structure, which has been solved at 2.2 Å resolution, includes residues 3–182 of two chains. Based on the evidence of dynamic light scattering experiments, this dimeric structure was considered as representative of the protein conformation in solution. Models of the mutants were built on the structure of wild-type ApoAI by manual residue replacement.

Molecular dynamics (MD) and trajectory analysis were performed with the software package GROMACS 4.6.6 [25–27] using the Gromos43a1 force field. Appropriate number of counterions (Na^+) was added to neutralize the systems. The structures were immersed in a rectangular box filled with SPC water molecules at a density of 1000 kg/m^3 [28] with periodic boundary conditions. Long-range electrostatic interactions were treated with the particle-mesh Ewald method with a grid spacing of 12 Å and cutoff of 8 Å. [29]. The molecules were submitted to initial energy minimisation with the steepest descent for 5000 steps followed by 500 ns NVT and 500 ps NPT equilibration with position restraints. Production runs were performed for 10 ns with a 2 fs step. To the best of our knowledge, these simulations are the first ever performed on mutants of ApoAI.

Temperature and pressure coupling were obtained with the v-rescale [30] and the Parrinello-Rahman [31] algorithms, respectively. Bond lengths were constrained using LINCS [32]. The overall flexibility of the systems was evaluated comparing the traces obtained by diagonalizing the covariance matrix of the coordinate fluctuations, as previously described [33]. Only Cα atoms were included in the definition of the covariance matrices. Figures were prepared with Pymol (www.pymol.org).

2.7. Complementary proteolysis experiments and mass spectrometry analysis

Complementary proteolysis experiments were carried out by treating 0.4 mg/mL solutions of proteins with trypsin, chymotrypsin, and endoproteinase Glu-C in 50 mM Tris HCl, pH 7.4. Different E:S ratios were optimized for each proteolytic probe as reported: 1:8000 for chymotrypsin and trypsin, 1:10,000 for endoprotease Glu-C. The extent of digestion was monitored on a time-course basis by sampling the reaction mixture at 15 and 30 min and blocking the reactions with 2% trifluoroacetic acid (TFA). Peptide mixtures were analyzed by liquid chromatography-mass spectrometry (LC–MS) onto a QuattroMicro LC-MS system (Micromass, Waters) interfaced with a 1100 HPLC (Agilent Technologies, Palo Alto, CA). Peptide mixtures from the different proteolysis experiments were fractionated by reverse-phase HPLC on a Phenomenex Jupiter C18 column (250 mm × 2.1 mm, 300 Å pore size) and eluted by using a step gradient from 5% to 60% of solvent B (5% formic acid and 0.05% TFA in acetonitrile) over 60 min and from 60% to 95% in 5 min (solvent A 5% formic acid and 0.05% TFA in water). The flow rate was kept at 200 μL/min and directly introduced in the mass spectrometers ESI source. Horse heart myoglobin was used to calibrate the instrument (average molecular mass 16,951.5 Da) at 5 scans/s.

2.8. Determination of critical concentration

Proteins were incubated at different concentrations (from 0.15 to 2 mg/mL) in 50 mM Tris HCl pH 7.4 for 14 days at 37 °C. Then, samples were centrifuged at 14,000 *g* for 30 min at r.t., supernatants were filtered with a 20 nm cut off filter and the absorbance at 280 nm measured.

2.9. Dynamic light scattering

Dynamic light scattering (DLS) measurements were carried out using a Malvern nano zetasizer (Malvern, UK) [34]. Proteins (0.55 mg/mL) were diluted in 50 mM Tris HCl at pH 7.4, filtered with a 0.22 μm cut off filter and incubated at 37 °C over time. Samples were placed in a disposable cuvette and held at 25 °C during analysis. The aggregation rate was monitored at time 0 and after 24 h, 48 h and 7 days of incubation. For each sample, spectra were recorded six times with 11 sub-runs using the multimodal mode. The Z average diameter was calculated from the correlation function using the Malvern technology software.

2.10. Atomic force microscopy

For AFM inspection, ApoAI samples were incubated at 0.3 mg/mL at 37 °C. Incubation times in the range from 4 to 7 weeks were considered. At the end of incubation, proteins were centrifuged at 1700 *g* for 10 min, the pellet was suspended in an equal volume of water, and a 10 μL aliquot was deposited on freshly cleaved mica and dried under mild vacuum. Tapping mode AFM images were acquired in air using a Multimode SPM, equipped with "E" scanning head (maximum scan size 10 μm) and driven by a Nanoscope V controller, and a Dimension 3100 SPM, equipped with a 'G' scanning head (maximum scan size 100 μm) and driven by a Nanoscope IIIa controller (Digital Instruments, Bruker AXS GmbH, Karlsruhe, Germany). Single beam uncoated silicon cantilevers (type OMCL-AC160TS, Olympus, Tokyo, Japan) were used. The drive frequency was between 290 and 340 kHz, the scan rate was between 0.3 and 0.8 Hz. Aggregate sizes were estimated from the heights in cross section of the topographic AFM images.

3. Results

3.1. Effects of amyloidogenic mutations on ApoAI secondary structure

The secondary structure content of AApoAI variants was estimated by far-UV CD spectroscopy at pH 7.4, at 0.15 mg/mL protein concentration to approximate physiological conditions. As shown in Fig. 1, wild-type ApoAI and the two amyloidogenic variant proteins were predominantly in an α-helical state, with a slightly lower α-helix content of the variants with respect to the wild-type protein (Table 1). When the proteins were incubated at 37 °C over time, no significant changes in the spectra of the wild-type protein were observed, consistently with literature data [18 and references therein]; on the contrary, the α-helicity of both variants decreased over time accompanied by an increase in β-strand, indicating an alteration of the protein native conformation towards an aggregation competent state.

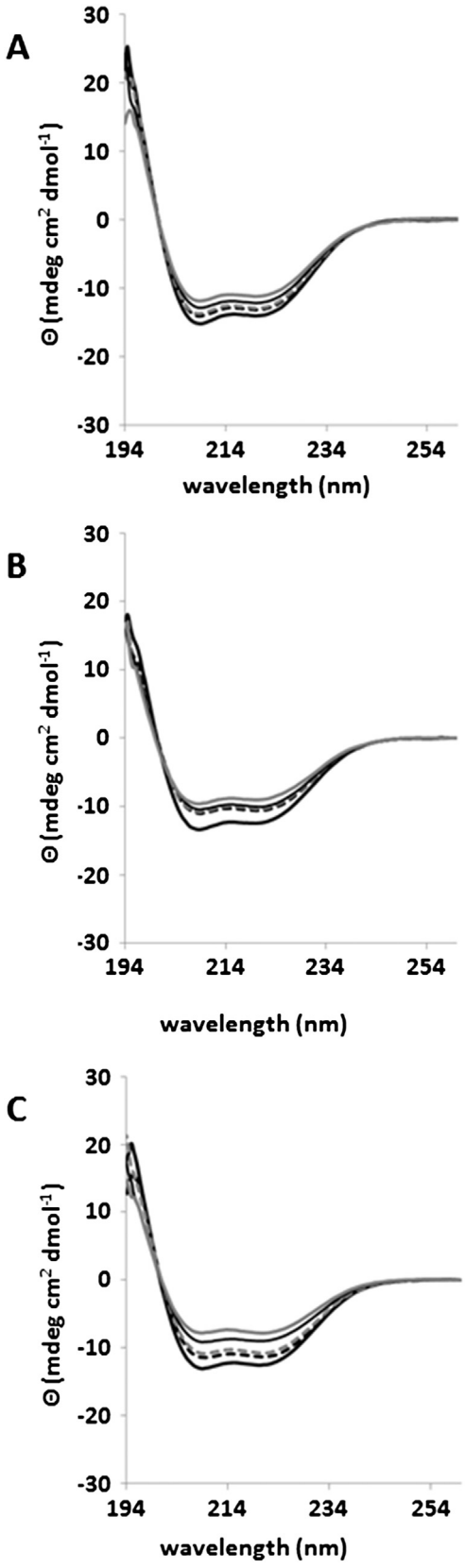

Fig. 1. Far-UV CD spectra of wild-type ApoAI and its amyloidogenic variants upon incubation at 37 °C. A, wild-type ApoAI; B, L75P-AApoAI; C, L174S-AApoAI. Spectra were acquired at 25 °C with 0.15 mg/mL protein concentration in 50 mM TrisHCl buffer, pH 7.4. Spectra were recorded at time 0 (bold black line), after 24 h (black dashed line), 48 h (gray dashed line), 72 h (black fine line) and after 7 days (bold gray line) incubation.

Table 1
α-Helix and β-strand contents (%) for wild-type ApoAI and its amyloidogenic variants, upon incubation at 37 °C. Data shown are the means from three independent experiments. The accuracy of the secondary structure content estimation is approximately 2% for wild-type ApoAI and 4% for its amyloidogenic variants.

Incubation time (h)	Wild-type ApoAI		L75P-AApoAI		L174S-AApoAI	
	α-Helix (%)	β-Strand (%)	α-Helix (%)	β-Strand (%)	α-Helix (%)	β-Strand (%)
0	49	29	40	36	45	28
24	49	28	34	36	40	21
48	47	29	32	39	35	37
72	40	34	31	39	29	41
168	38	33	29	40	20	53

3.2. Effects of amyloidogenic mutations on ApoAI conformation

During amyloid formation protein aggregation leads to an increase in the exposure of hydrophobic regions to the aqueous environment. ANS binding studies revealed a 3-fold increase of ANS fluorescence intensity in the presence of wild-type ApoAI (Fig. 2A, black line), due to the exposure of ANS accessible hydrophobic surfaces, as previously reported [35–38]. A larger increase of ANS fluorescence was measured for both variants compared to wild-type ApoAI, particularly evident for L174S-AApoAI variant, indicating that both mutations trigger the exposure of hydrophobic regions (Fig. 2A, gray line and dashed line for L75P-AApoAI and L174S-AApoAI, respectively).

To compare the tertiary structure of AApoAI variants with that of the wild-type protein, the intrinsic fluorescence emission intensity was registered and the shift of maximum emission wavelength (λ_{max}), due to changes in solvent exposure of tyrosine and tryptophan residues, was evaluated. As the four Trp residues of the wild-type protein (at positions 8, 50, 72 and 108), as well as the five Tyr residues (at positions 18, 29, 100, 115, 166), are located within the four-helix bundle domain and are all conserved in the amyloidogenic variants under study, this analysis is a measure of the stability of AApoAI N-terminal region. Fluorescence spectra were collected either upon excitation at 295 nm, where the contribution of tyrosine residues is negligible (Fig. 2B), or upon excitation at 280 nm, where both Tyr and Trp residues significantly contribute to the absorption (Fig. 2C). As shown in Fig. 2B, in the case of L75P-AApoAI (gray line) the maximum fluorescence intensity emission wavelength ($\lambda_{max} = 344.7 \pm 0.3$ nm) is higher than that of wild-type ApoAI ($\lambda_{max} = 335.7 \pm 0.6$ nm). These data suggest that the substitution L75P is able to induce changes in the conformation of the N-terminal domain with consequent exposure of hydrophobic protein surfaces, since proline is known to interrupt protein α-helical structure. On the contrary, L174S-AApoAI (Fig. 2B, dashed line) showed a $\lambda_{max} = 336.3 \pm 1.2$ nm, a value similar to that recorded for wild-type ApoAI. Similar results were observed when the contribution of both Tyr and Trp was analyzed (Fig. 2C and Table S1).

3.3. Effects of mutations on ApoAI stability

To get insights into the structural features that favor AApoAI amyloidogenicity, we compared the folding of the L75P-AApoAI and L174S-AApoAI to that of wild-type ApoAI by investigating protein stability in the presence of chemical denaturing agents, such as guanidine hydrochloride (GdnHCl) and urea. Upon excitation at 295 nm, the unfolding transition was monitored by evaluating the change in λ_{max} as a function of chemical agent concentration. As the equilibrium unfolding of wild-type ApoAI by GdnHCl has been well characterized, it can be used as a reference for the stability of the variants. As shown in Fig. 3(A–B), sigmoidal curves (filled squares) were obtained in the case of wild-type protein, confirming a cooperative unfolding pattern that well fits the two-state model [18,39]. As shown in Table 2, the mid-point of the denaturation process ($D_{1/2}$ values), ΔG_D° and

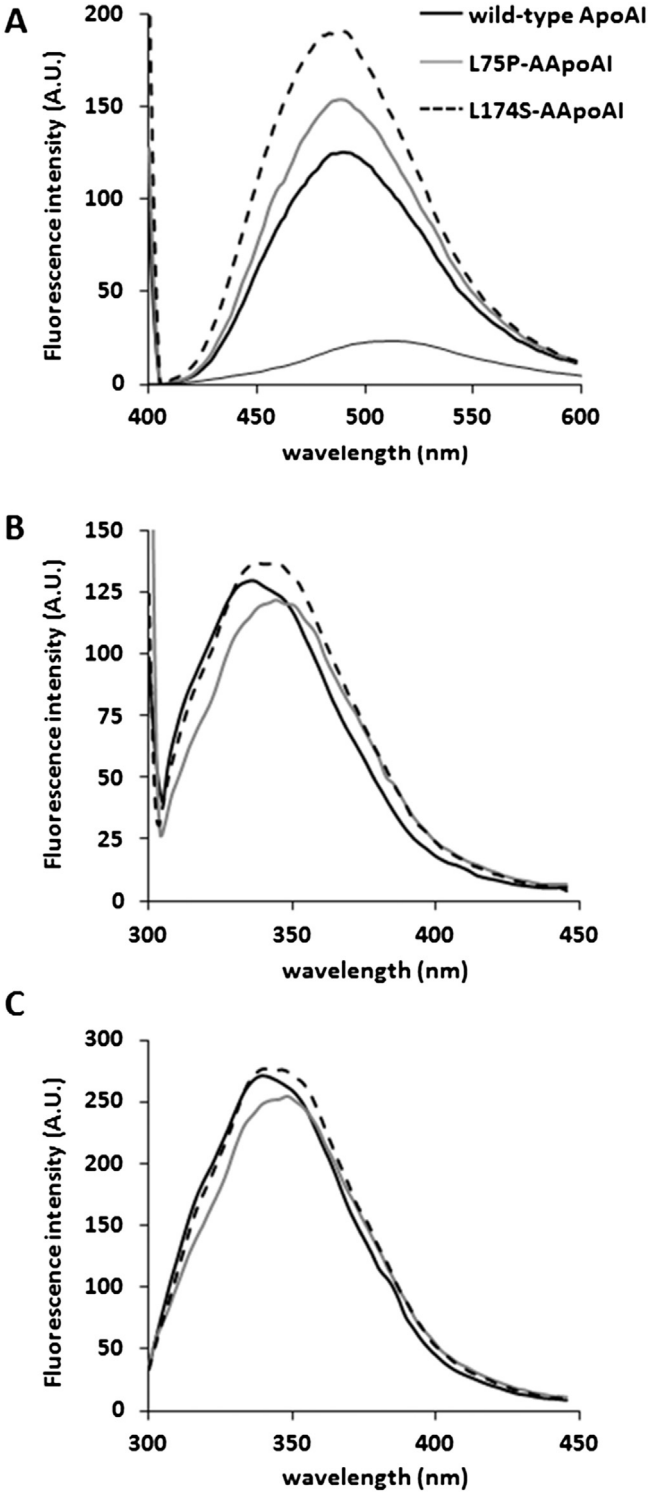

Fig. 2. Fluorescence analyses of AApoAI variants. A, binding of ANS to wild-type ApoAI (black line) and to its amyloidogenic variants L75P (gray line) and L174S (dashed line). ANS spectrum is reported as a fine black line. ANS emission fluorescence spectra were recorded in the range from 400 to 600 nm at the excitation wavelength of 395 nm. ANS emission was monitored at pH 7.4. B and C, tryptophan and tyrosine emission spectra at pH 7.4 of wild-type ApoAI (bold black line), L75P-AApoAI (gray line) and L174S-AApoAI (dashed line). Fluorescence was excited at 295 nm (B) and at 280 nm (C).

cooperativity (m) values were similar to those previously reported [18 and references therein].

A completely different behavior was observed in the case of L75P-AApoAI and L174S-AApoAI, as the denaturation curves are shifted to lower denaturant concentrations compared to wild-type ApoAI, indicating a decreased structural stability. In particular, for L75P-AApoAI variant (empty circles in Fig. 3 (A–B), protein unfolding was found not to be a cooperative process and a higher λ_{max} was recorded even in the absence of the denaturing agent. On the other hand, for

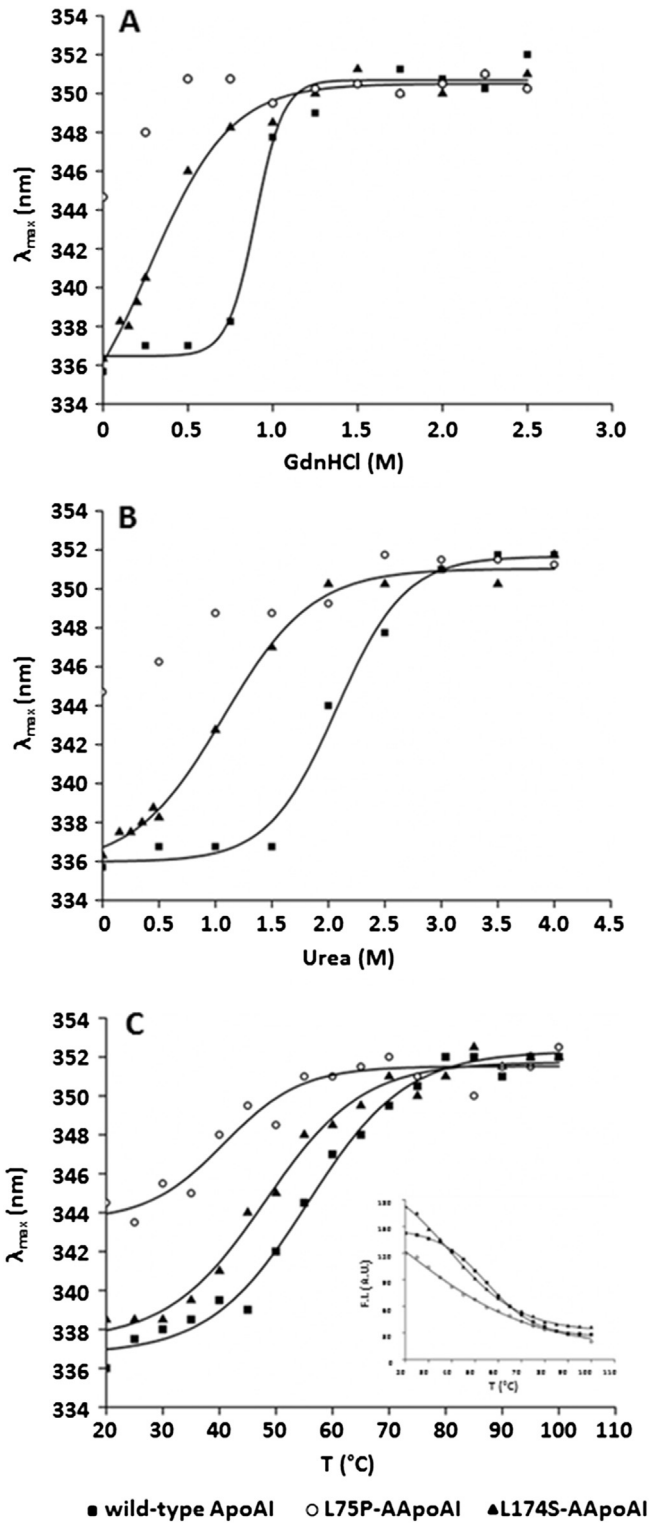

Fig. 3. Unfolding of wild-type ApoAI (filled squares) and of its amyloidogenic variants L75P (empty circles) and L174S (filled triangles) induced by the addition of increasing amounts of GdnHCl (A), urea (B), or by temperature changes (C). Following excitation at 295 nm, emission spectra were recorded and curves were obtained by reporting the maximum emission fluorescence as a function of the denaturing agent concentration value. Tryptophan fluorescence intensity as a function of temperature is reported as an inset in C.

Table 2
Denaturation parameters for the unfolding of AApoAI variants. Data shown are the means from three independent experiments.

Protein	$D_{1/2}$ (M)	ΔG_D° (kcal/mol)	m	$D_{1/2}$ (M)	ΔG_D° (kcal/mol)	m	Tm (°C)	ΔH (kcal/mol)
	GdnHCl			Urea			Temperature	
Wild-type ApoAI	0.90 ± 0.01	2.9 ± 0.5	2.76 ± 0.32	2.1 ± 0.3	4.4 ± 0.4	2.0 ± 0.1	55.3 ± 0.5	26.9 ± 0.1
L75P-AApoAI	n.a.	n.a.	n.a.	n.a.	n.a.	n.a.	40.8 ± 2.2	15.0 ± 0.4
L174S-AApoAI	0.39 ± 0.01	0.20 ± 0.04	0.9 ± 0.2	1.1 ± 0.4	1.3 ± 0.2	1.0 ± 0.2	43.5 ± 4.6	22.4 ± 0.4

L174S-AApoAI variant, a hyperbolic curve (filled triangles in Fig. 3A) was obtained in the presence of GdnHCl, indicative of a fast and non-cooperative unfolding process. Following the addition of increasing amounts of urea, a sigmoidal curve was obtained for L174S variant (Fig. 3B, filled triangles) even though less pronounced when compared to the wild-type protein, indicating a loss in unfolding cooperativity. Denaturation parameters for the unfolding process of AApoAI variants are reported in Table 2. The lower GdnHCl $D_{1/2}$ values obtained for wild-type ApoAI and L174S variant, compared to urea $D_{1/2}$, may suggest the importance of electrostatic interactions, efficiently weakened by GdnHCl, in the stabilization of the two proteins [40]. Loss in cooperativity during denaturation is a common feature of amyloidogenic variants, as variants G26R and L178H [18], and the recently published R173P [20] share this behavior.

Finally, by thermal denaturation (Fig. 3C) we observed that the proteins are all structurally stable up to 50 °C, although enthalpy and midpoint values, reported in Table 2, were found to be lower for the variants than for wild-type ApoAI, confirming their lower stability with respect to the native protein.

3.4. Structural features of wild-type ApoAI, L75P-AApoAI and L174S-AApoAI: a molecular dynamics study

To address differences in the structural features of the two variants when compared to the wild-type protein, models of the variants were obtained and used as inputs for a molecular dynamics (MD) study. In wild-type ApoAI, L75 is located in the middle of the short helix 70–76 that contributes to define the relative helical orientation in the four-segment bundle and interacts with L14 in the "bottom" hydrophobic cluster formed by V11, L14, F71 and L82. L174, instead, is located in the packed "bottom" hydrophobic cluster so that its substitution with Ser was expected to disrupt this cluster [17,22]. On the other hand, from the MD simulations it emerged that the replacement of L174 with a Ser has only a moderate effect on the overall structure of the protein. In fact, in the L174S variant, the serine side chain can be well accommodated within the helix 141–180, since it can form a hydrogen bond with the carbonylic oxygen of Y170 (Fig. 4A). On the contrary, the L75P substitution has a stronger destabilizing effect, since the presence of Pro breaks helix 70–76 and disturbs the stabilizing hydrophobic interactions that play a major role in orienting the helices of the four-segment bundle (Fig. 4B).

During the MD simulations, no significant changes in the overall structure from the corresponding crystal structure occurred in wild-type ApoAI, while the two variants show subtle, but significant variations. In particular, the average structures extracted from the trajectories for the three proteins suggest that L174S-AApoAI, which has an overall structure similar to that of wild-type protein, presents a slight reduced radius of gyration (5.91 ± 0.02 nm vs 5.98 ± 0.03 nm of wild-type ApoAI), while L75P-AApoAI adopts a less compact structure (+2% in the total solvent accessible surface area), with a significant loss of α-helical content (about −2%). These differences well reflect in the average distances between donor and acceptor atoms involved in the formation of 3_{10}-, α- and π-helices (Table S2). These data are in overall agreement with those obtained by CD spectra (Fig. 1).

To verify if the conformational changes induced by the mutations also affects the overall dynamics of the proteins, the trace of the covariance matrix of CA atoms for the three structures, which is a measure of the overall flexibility [33], has been evaluated. The values for wild-type ApoAI, L75P-AApoAI and L174S-AApoAI were 75 nm^2, 105 nm^2 and 98 nm^2, respectively. These data clearly indicate that the mutations enhance the overall flexibility of the protein.

To obtain a more detailed picture of the observed differences, the percentage of α-helical content of each residue (helicity) during the simulation was plotted as a function of the residue number (Fig. S1). Interestingly, although the plots have an overall similar profile for the three proteins, some differences can be evidenced: wild-type ApoAI is generally more structured; however in the regions encompassing residues 18–30, 80–81 and 126–131 it is slightly less structured than the two variants. L75P-AApoAI shows a lower helical content in correspondence of residues 66–73, 135–137, 157–160 and 172–177, but it is more structured than both wild-type ApoAI and L174S in the regions 125–129 and 140–142. L174S-AApoAI has a lower α-helical content in correspondence of residues 107–110, 140–141, but it is more structured in the regions 77–80 and 158–160. These differences are associated with slight variations also in the solvent accessible surface area per residue. Notably, although in the L75P variant the region encompassing residues 135–137 presents a lower helical content when compared to the other proteins (Fig. S1), it becomes more buried than in L174S-AApoAI and the wild-type protein, as the average solvent accessible surface area of residue 136 is: 76, 62 and 76 $Å^2$, in wild-type, L75P-AApoAI and L174S-AApoAI, respectively.

3.5. Complementary proteolysis experiments

In order to define ApoAI regions structurally altered by the presence of mutations, the surface topology of wild-type protein, L75P-AApoAI and L174S-AApoAI variants was investigated by a complementary proteolysis approach coupled with mass spectrometry identification of cleavage sites (LC–MS) [41]. Complementary proteolysis refers to limited proteolysis experiments carried out in conditions able to generate a single proteolytic event on the protein which originates two "complementary" peptides. Further cleavages occurring on the two complementary peptides are not considered. Conformational changes induced by mutations and affecting protein topology were monitored by the appearance of preferential cleavage sites located in exposed and flexible regions of the proteins, which become more susceptible to proteolysis [42,43]. Complementary proteolysis experiments were performed using trypsin, chymotrypsin and endoprotease Glu-C as conformational probes. All reactions were carried out in parallel on the three proteins by using the same E:S ratio and were monitored on a time-course basis by sampling the incubation mixture after 15 and 30 min of hydrolysis. Following this time course approach, primary and secondary cleavage sites, always produced by a single proteolytic event, were only defined on kinetic basis. The LC–MS profiles showed that both variants were more susceptible to proteases than the wild-type protein, as demonstrated by the higher number of peptides released at the same hydrolysis time (data not shown). This observation suggests that both AApoAI variants are more flexible and/or less structured than the wild-type protein, in agreement with both spectroscopic and molecular dynamics data.

The distribution of the proteolytic sites is outlined in Fig. 4C. A similar pattern of proteolytic accessibility could be observed in all the

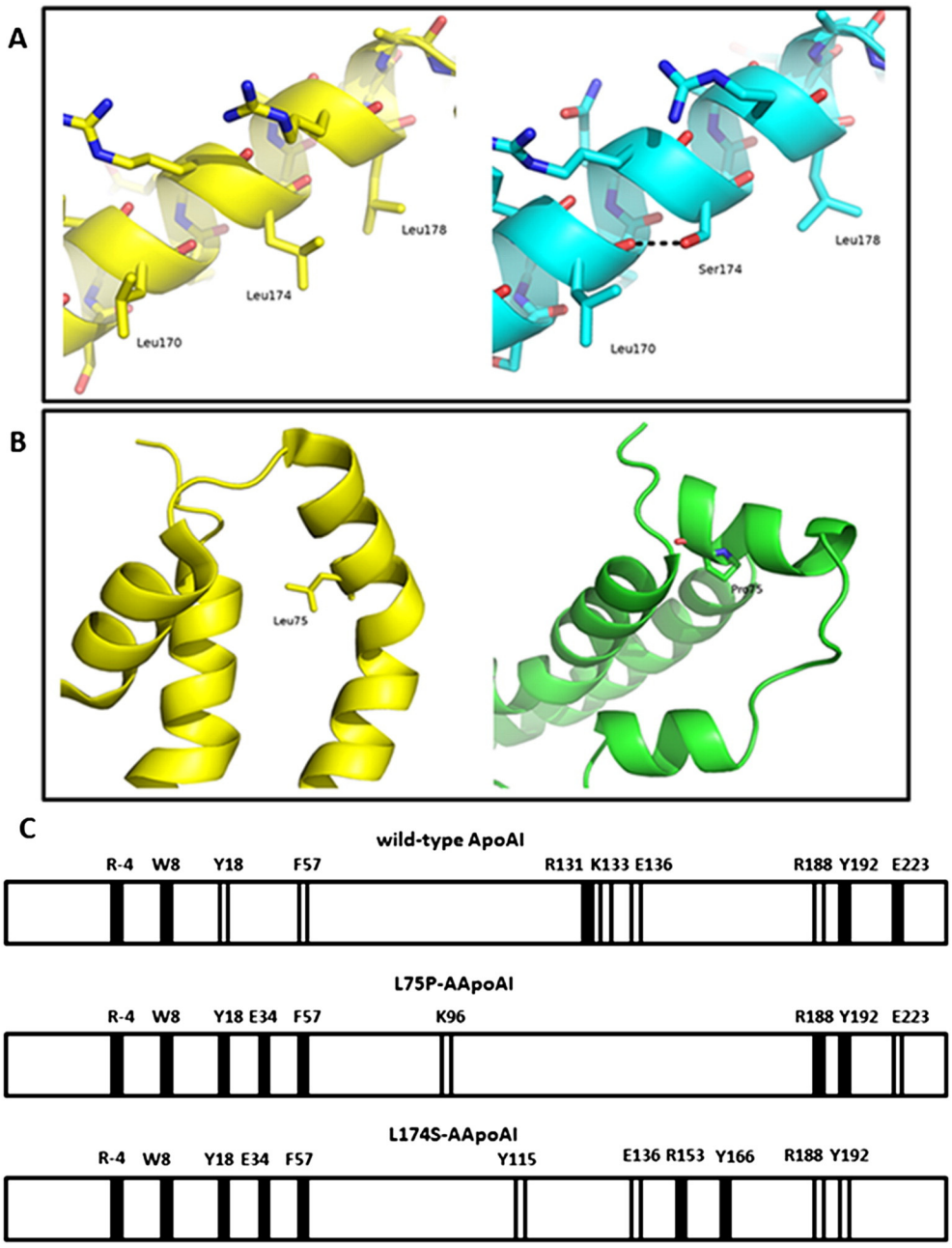

Fig. 4. Structural features of AApoAI variants. A, insight of the structure of helix encompassing residues 141–180 in wild-type ApoAI (yellow) and in L174S variant (cyan). B, ribbon representation of the helix bundle in proximity of L75 in the structure of wild-type ApoAI (yellow) and of L75P variant (green). For sake of clarity, one helix from the second chain of the dimer was removed. C, pattern of preferential proteolytic sites in native and AApoAI variants. Schematic representation of the results obtained from limited proteolysis experiments on wild-type ApoAI (upper), L75P-AApoAI (middle) and L174S-AApoAI (lower). Proteolytic sites are designed as primary (filled) or secondary sites (empty) merely on kinetic basis. The R-4 cleavage site was not taken in consideration, as it is located in the his-tag peptide sequence occurring in the recombinant proteins.

proteins, with preferential cleavage sites gathering at both the N- and C-terminal regions. However, hydrolysis at Y18 and F57 occurred much faster in the mutants than in wild-type ApoAI and E34 was not recognized in the native protein, suggesting a higher flexibility in the N-terminal region of the variants. Moreover, cleavage at K96 and Y115, in L75P- and L174S-AApoAI, respectively, suggests a slight conformational change in the region including the putative proteolytic site in AApoAI variants, responsible for the release of the fibrillogenic polypeptide. On the contrary, in wild-type ApoAI this region, as reported in the crystal structure [17], is in a predominantly α-helical structure, which protects the protein from proteolytic cleavage.

Also at the C-terminus, wild-type ApoAI and L75P variant are characterized by a quite similar proteolytic profile, showing accessibility at residues R188, Y192 and E223. This region seems to be protected in the L174S variant, as showed by the disappearance of the E223 cleavage site and by a slower kinetic of hydrolysis at level of R188 and Y192 residues, thus suggesting that a slight conformational change occurred in this region. Further differences in the proteolytic patterns of the three proteins were located in the region encompassing the 131–136 sequence that was exposed in the wild-type ApoAI, as demonstrated by cleavages at R131, K133 and E136. On the contrary, this region became completely inaccessible in the L75P variant, in perfect agreement with the molecular dynamics simulation. The accessibility of this sequence changed also in the L174S variant, where E136 was still recognized, but with slow kinetics and the appearance of new cleavage sites at R153 and Y166 was detected. It is noteworthy that these cleavages occurred quite close to the mutation site 174, indicating a higher accessibility of this region, as suggested by molecular dynamics calculations.

From MD and complementary proteolysis experiments we can conclude that both L75P- and L174S-AApoAI variants have an increased exposure of the N-terminal region.

3.6. Effects of mutations on ApoAI aggregation

As structural and conformational alterations have been associated with the presence of a single point mutation, the impact of pathogenic substitutions on the aggregation propensity of full-length AApoAI was investigated by using different approaches. First, to get information about the critical concentration [44] of AApoAI variants, proteins were incubated at different concentrations for 14 days at 37 °C. Their final concentration (c_f) was measured spectrophotometrically following the removal of aggregated species, as described in the Methods section. In the graph (Fig. S2), we reported $1 - c_f / c_i$ versus c_i, where c_i is the initial protein concentration and $1 - c_f / c_i$ is a measure of protein aggregated species. We calculated a critical concentration of 0.18 ± 0.05 mg/mL for L75P variant and 0.15 ± 0.04 mg/mL for L174S variant. No aggregation occurred for the wild-type protein.

Next, we measured the kinetics of aggregation of AApoAI variants by ThT binding assays. Proteins were incubated (0.3 mg/mL) at pH 7.4 in the presence of ThT, and the increase of ThT emission fluorescence at 482 nm was measured over time (Fig. 5A). A much higher increase in ThT fluorescence intensity was observed in the case of L174S-AApoAI variant with respect to L75P-AApoAI, whereas no aggregation of the wild-type protein was observed, in line with previous results [18]. For both AApoAI variants, a double-sigmoidal curve of ThT emission was observed, less evident in the case of L75P-AApoAI variant (inset of Fig. 5A). For both variants, the first transition occurred with a smaller amplitude increase in ThT fluorescence intensity with respect to the second one. The apparent $t_{1/2}$ values were: 29 ± 9 h and 96 ± 10 h for L75P-AApoAI and 35 ± 6 h and 83 ± 7 h for L174S-AApoAI. In agreement with data reported by Grudzielanek and coworkers on insulin aggregation [45], we hypothesize that the first transition is associated to with the formation of partially folded species able to bind ThT, whereas the second transition can be due to the formation of amyloid nuclei (Fig. 5A). Similar results were obtained in the presence of physiological amount of NaCl (0.15 M). Hence, in our experimental conditions, low salt concentration has no significant effect on the aggregation propensity of AApoAI variants.

Then, we analyzed the stability of protein tertiary structure upon incubation at 37 °C, as destabilization represents a crucial step during fibrillogenesis [46]. Proteins were incubated at 37 °C up to 1 week and at time intervals ANS binding experiments and intrinsic fluorescence analyses were performed (Fig. S3). In the presence of either amyloidogenic variants an increase in ANS fluorescence, more evident for L174S-AApoAI (Fig. S3C, gray line), was detected after 72 h, suggesting conformational changes leading to the exposure of hydrophobic surfaces. A decrease in ANS binding was observed after a prolonged incubation (1 week, Fig. S3C, dashed lines), suggesting shielding of hydrophobic patches due to their direct involvement in fibril formation. No changes in ANS binding was observed instead in the case of wild-type ApoAI (Fig. S3A). These results were confirmed by intrinsic fluorescence experiments (Fig. S3D–I and Table S1), showing a decrease of the emission maximum after 72 h incubation to be related to protein aggregation. As a consequence, Trp residues are hindered and remain buried instead of being exposed to the solvent.

Furthermore, we evaluated the apparent hydrodynamic diameter of the three proteins by means of dynamic light scattering (DLS). For wild-type ApoAI we obtained an apparent hydrodynamic diameter of 11.0 ± 1.1 nm, consistent with the size of a protein dimer, as previously reported by X-ray crystallography [22]. The hydrodynamic diameter of the

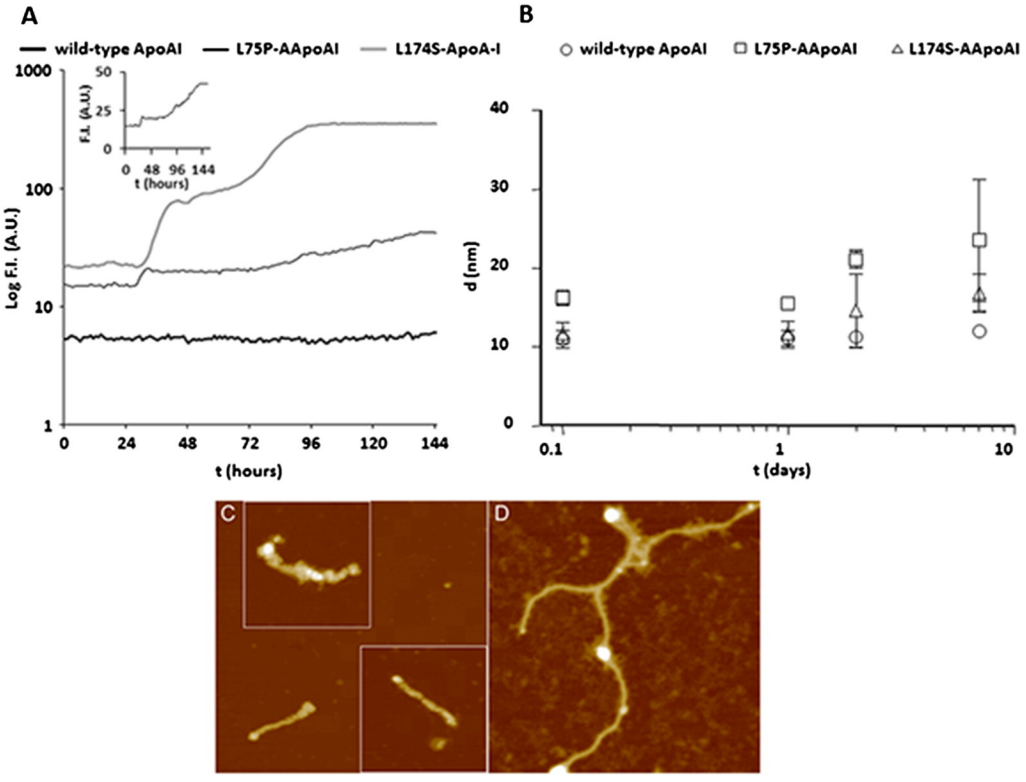

Fig. 5. AApoAI aggregation. A, ThT binding assay. Proteins under test were incubated for 144 h at 25 °C in 50 mM Tris HCl, pH 7.4. During the incubation, emission fluorescence values at 482 nm were recorded every 60 min. A typical curve for wild-type ApoAI (black bold line), L75P-AApoAI (black fine line) and L174S-AApoAI (gray bold line) are shown. The inset shows an enlargement of L75P-AApoAI curve. B, apparent hydrodynamic diameter of AApoAI variants over time. Wild-type ApoAI (empty circles), L75P-AApoAI (empty squares) and L174S-AApoAI variant (empty triangles) were incubated at 37 °C for different length of time. The hydrodynamic diameter, d (nm), is reported as a function of time, t (days), expressed as logarithm of time. C, D, tapping mode AFM images (height data) of L75P-AApoAI (C) and L174S-AApoAI (D) aggregates obtained after seven weeks incubation. Scan size 750 nm, Z range 29 nm (C and insets), 12 nm (D). The insets in C are at the same scale of the background image (inset scan size, 500 nm).

L174S-AApoAI variant was 11.8 ± 1.4 nm, similar to the value obtained for the wild-type protein, whereas the L75P-AApoAI variant showed a diameter of 16.3 ± 0.9 nm, consistent with a less-compact structure than the native protein, according to intrinsic fluorescence experiments and MD simulations (Fig. 2B-C). When proteins were analyzed after 24 h incubation, no formation of higher molecular aggregated species were detected in the three samples, as indicated in Fig. 5B, where the diameter values are plotted as a function of the incubation time. Indeed, wild-type ApoAI showed a constant apparent diameter up to 7 days (Fig. 5B) in agreement with ANS binding experiments, intrinsic fluorescence analyses and ThT binding (Figs. 2 and 5A), thus confirming no aggregation for the wild-type protein. On the contrary, the variants showed a different behavior with respect to ApoAI, with peculiar characteristics differentiating one from the other. The apparent diameter of L174S-AApoAI gradually increased up to 16.9 ± 2.4 nm after 7 days incubation, whereas L75P-AApoAI reached an apparent diameter value of 23.6 ± 7.8 nm, suggesting a pronounced decrease of protein compactness over time.

Finally, AFM experiments were performed to inspect the aggregate morphology after incubation times ranging from 4 to 7 weeks. We found that L75P-AApoAI formed scanty, short fibrils with length of 200–350 nm and height of 4–6 nm (Fig. 5C). These fibrils exhibit a beaded morphology, resulting from the assembly of different subunits of variable size, with not very regular packing. The L174S-AApoAI variant displayed a higher density of fibrillar aggregates as compared to L75P-AApoAI. These aggregates were generally smoother, longer and thinner than those formed by L75P-AApoAI, exhibiting typical lengths between 200 nm and 4 μm and heights between 1 and 3 nm; Fig. 5D shows L174S-AApoAI fibrils detected after 7 weeks incubation. In addition, a minority of thick, beaded fibrils (length 400–500 nm, height 5–6 nm) was also observed (not shown). No fibrils were detected for wild-type ApoAI in the same conditions. All the data collected indicate that the AApoAI variants are prone to aggregate and generate fibrils qualitatively similar to the fibrillar structures reported in the literature for other AApoAI variants [18,19].

4. Discussion

Using an array of independent methodologies, the effects of the "inside mutation" L75P and the "outside mutation" L174S on ApoAI propensity to undergo an amyloidogenic pathway have been analyzed with the aim of elucidating common and different features of amyloidogenic mutations in the development of the disease. We found that both variants display: (i) a slightly lower α-helical content with respect to the native protein and a time dependent increase of β-strand structure; (ii) more exposed hydrophobic regions, particularly evident for L174S variant; (iii) reduced stability and loss of unfolding cooperativity; (iv) increased flexibility; and (v) enhanced susceptibility to protease cleavage in the N-terminal region.

Nevertheless, the two variants show significant differences, which contribute to add knowledge to the emerging picture of the cause and effect relationship in ApoAI associated amyloidosis. As supposed, the substitution of L75 with proline has a destabilizing effect, as it breaks helix 70–76. This helix overlaps with one of the three predicted N-terminal amyloid "hot spots", whose perturbation has been recently suggested to be a prerequisite for misfolding [21]. This leads to the exposure of hydrophobic residues mainly located in the N-terminal region, as demonstrated by the increased intrinsic fluorescence intensity and ANS binding, as well as by the exposure of a proteolytic site at Y18, belonging to the major hot spot 14–22, as also found for G26R and L178H variants [18]. Furthermore, the accessibility of further proteolytic sites at E34 and F57 (the latter belonging to the minor hot spot 53–58), both hindered in the native protein, is the consequence of the propagation of the local perturbation (helix 70–76) to the other two predicted hot spots and the cause of the decreased protein compactness. In fact, DLS measurements of the hydrodynamic diameter demonstrated that the L75P variant is a much less compact protein with respect to both the wild-type protein and the L174S variant, with an increased diameter of 50%. Therefore, as a response to the occurrence of the "internal" mutation L75P, the protein acquires a "looser" structure at the N-terminal domain, with significant alteration of protein conformation and compactness, while the "external" mutation L174S is responsible for a less destabilized but more flexible structure to which a more pronounced aggregation-competent state is associated.

In the 3D structure, residue 174 is in close proximity to hot spot 14–22 which appears to be destabilized, as indicated by the appearance of a cleavage site at Y18. This perturbation could affect the hot spot 53–58, in line with cleavage at F57. Moreover, in the L174S variant cleavages at R153 and Y166 occur. The structural differences between L75P- and L174S-AApoAI variants are mainly due to differences in the exposed regions of the proteins. We believe that in L75P variant the N-terminal region is more unstructured, as indicated by Trp intrinsic fluorescence (Fig. 2B) and suggested by DLS measurements (Fig. 5B) and MD simulations (Fig. 4B), whereas in L174S the region encompassing residues 153–166 seems to be more unstructured, as demonstrated by limited proteolysis experiments (Fig. 4C).

We propose that these structural features represent the molecular basis of the different aggregation propensity of the two variants. Following incubation at 37 °C, L174S shows a higher propensity to aggregate than the L75P variant, as demonstrated by CD and fluorescence analyses, ThT binding and AFM imaging. The time-dependent increase of β-sheet structure, shown by L75P and L174S variants, is similar to that of G26R-AApoAI [18], whereas for L178H-AApoAI an increase in the α-helical content has been described over time, accompanied by the formation of very short fibrillar structures [18]. Upon 7 days incubation at 37 °C, DLS measurements revealed an over time increase of protein diameter by about 50% and 44% for the L75P and L174S variants, respectively, compared to the wild-type protein. Noteworthy, L75P-AApoAI lower compactness well correlates with the beaded morphology of its fibrils, whereas even though L174S-AApoAI is relatively compact and less unstructured than the other variant, it presents higher aggregation propensity than L75P-AApoAI. It is likely that in this case a balance between protein compactness, partial unfolding, group exposure and flexibility regulates protein amyloidogenicity.

Our data indicate that both amyloidogenic mutations induce protein destabilization in a region close to the mutated residue. The propagation of the destabilization to the N-terminal hot spots region, allowed by their proximity in the 3D structure, is a sine qua non condition for aggregation, as recently suggested by Das and coworkers [21]. The polymorphic behavior observed in our experimental system is not surprising, as polymorphism is a common feature of amyloid aggregation; in this case it could be also favored by the direct involvement of the N-terminal region alone in triggering aggregation, thus resulting in possible multiple arrangements of the rest of the protein.

Differently from the accepted pathway in which AApoA-I is cleaved prior to aggregation, Das and coworkers [21] suggested that AApoAI cleavage can occur only after aggregation of the full-length protein. Therefore, aggregation of the N-terminal region of the full-length protein would represent the first step in the fibrillogenic process. Following the specific cleavage of the full-length variant, the formation of mature fibrils could be observed. Our observation that L75P- and L174S-AApoA-I are able to aggregate as full-length proteins is consistent with this model, and the scantiness of mature fibrils can be explained by the lack of the proteolytic cleavage. Our findings highlight a potential key element in the evolution of the disease, i.e. the partial exposure of K96 and Y115 cleavage sites in L75P- and L174S-AApoAI, respectively. In fact, in this region, which is fully hindered in the native protein, the cleavage sites that allow the release of the fibrillogenic N-terminal polypeptide(s) are expected to be present. It is tempting to speculate that this region becomes fully exposed upon aggregation of the full-length variants.

In conclusion, our study adds knowledge, at a molecular level, to the general mechanism by which amyloidogenic mutations determine

ApoAI systemic amyloidosis, providing a new *tessera* in the puzzle of such a severe disease.

Supplementary data to this article can be found online at http://dx.doi.org/10.1016/j.bbagen.2015.10.019.

Author contribution

R.D.G and D.M.M. conceived the experiments; F.I. and R.D.G. constructed mutants; G.P. express and purified recombinant proteins; R.D.G. performed the biochemical experiments; M.M. and D.C. carried out proteolysis experiments; M.B. performed DLS experiments; A.M. performed the MD analyses; A.P. performed the AFM experiments; R.D.G., D.M.M., A.A., A.R., S.M.M., R.P. and P.P. analyzed the results; R.D.G., and D.M.M. wrote the paper with the contribution of all authors.

Funding

The authors thank the Italian MIUR (Ministero dell'Università e della Ricerca Scientifica, Progetti di Rilevante Interesse Nazionale) Project (PRIN 2009STNWX3) and the University of Genoa (Projects PRA2013 and PRA2014) for the financial support to the activities reported in the present study.

Transparency document

The Transparency document associated with this article can be found, in the online version.

References

[1] M. Eriksson, S. Schonland, S. Yumlu, U. Hegenbart, H. von Hutten, Z. Gioeva, P. Lohse, J. Büttner, H. Schmidt, C. Röcken, Hereditary apolipoprotein AI-associated amyloidosis in surgical pathology specimens: identification of three novel mutations in the APOA1 gene, J. Mol. Diagn. 11 (2009) 257–262.
[2] A. Relini, S. Torrassa, R. Rolandi, A. Gliozzi, C. Rosano, C. Canale, M. Bolognesi, G. Plakoutsi, M. Bucciantini, F. Chiti, M. Stefani, Monitoring the process of HypF fibrillization and liposome permeabilization by protofibrils, J. Mol. Biol. 338 (2004) 943–957.
[3] P. Westermark, M.D. Benson, J.N. Buxbaum, A.S. Cohen, B. Frangione, S. Ikeda, C.L. Masters, G. Merlini, M.J. Saraiva, J.D. Sipe, A primer of amyloid nomenclature, Amyloid 14 (2007) 179–183.
[4] S.T. Ferreira, F.G. De Felice, A. Chapeaurouge, Metastable, partially folded states in the productive folding and in the misfolding and amyloid aggregation of proteins, Cell Biochem. Biophys. 44 (2006) 539–548.
[5] S.T. Ferreira, M.N. Vieira, F.G. De Felice, Soluble protein oligomers as emerging toxins in Alzheimer's and other amyloid diseases, IUBMB Life 59 (2007) 332–345.
[6] K.A. Rye, P.J. Barter, Formation and metabolism of prebeta-migrating, lipid-poor apolipoprotein A-I, Arterioscler. Thromb. Vasc. Biol. 24 (2004) 421–428.
[7] G. Cavigiolio, E.G. Geier, B. Shao, J.W. Heinecke, M.N. Oda, Exchange of apolipoprotein A-I between lipid-associated and lipid-free states: a potential target for oxidative generation of dysfunctional high density lipoproteins, J. Biol. Chem. 285 (2010) 18847–18857.
[8] L. Obici, G. Franceschini, L. Calabresi, S. Giorgetti, M. Stoppini, G. Merlini, V. Bellotti, Structure, function and amyloidogenic propensity of apolipoprotein A-I, Amyloid 13 (2006) 1–15.
[9] D. Rowczenio, A. Dogan, J.D. Theis, J.A. Vrana, H.J. Lachmann, A.D. Wechalekar, J.A. Gilbertson, T. Hunt, S.D. Gibbs, P.T. Sattianayagam, et al., Amyloidogenicity and clinical phenotype associated with five novel mutations in apolipoprotein A-I, Am. J. Pathol. 179 (2011) 1978–1987.
[10] M. Gomaraschi, L. Obici, S. Simonelli, G. Gregorini, A. Negrinelli, G. Merlini, G. Franceschini, L. Calabresi, Effect of the amyloidogenic L75P apolipoprotein A-I variant on HDL subpopulations, Clin. Chim. Acta 412 (2011) 1262–1265.
[11] L. Obici, G. Palladini, S. Giorgetti, V. Bellotti, G. Gregorini, E. Arbustini, L. Verga, S. Marciano, S. Donadei, V. Perfetti, et al., Liver biopsy discloses a new apolipoprotein A-I hereditary amyloidosis in several unrelated Italian families, Gastroenterology 126 (2004) 1416–1422.
[12] P. Mangione, M. Sunde, S. Giorgetti, M. Stoppini, G. Esposito, L. Gianelli, L. Obici, L. Asti, A. Andreola, P. Viglino, et al., Amyloid fibrils derived from the apolipoprotein A1 Leu174Ser variant contain elements of ordered helical structure, Protein Sci. 10 (2001) 187–199.
[13] C.L. Murphy, S. Wang, K. Weaver, M.A. Gertz, D.T. Weiss, A. Solomon, Renal apolipoprotein A-I amyloidosis associated with a novel mutant Leu64Pro, Am. J. Kidney Dis. 44 (2004) 1103–1109.
[14] R. Del Giudice, D.M. Monti, C. Sarcinelli, A. Arciello, R. Piccoli, G.F. Hu, Amyloidogenic variant of apolipoprotein A-I elicits cellular stress by attenuating the protective activity of angiogenin, Cell Death Dis. 5 (2014), e1097.
[15] M. Marchesi, C. Parolini, C. Valetti, P. Mangione, L. Obici, S. Giorgetti, S. Raimondi, S. Donadei, G. Gregorini, G. Merlini, et al., The intracellular quality control system down-regulates the secretion of amyloidogenic apolipoprotein A-I variants: a possible impact on the natural history of the disease, Biochim. Biophys. Acta 1812 (2011) 87–93.
[16] A. Andreola, V. Bellotti, S. Giorgetti, P. Mangione, L. Obici, M. Stoppini, J. Torres, E. Monzani, G. Merlini, M. Sunde, Conformational switching and fibrillogenesis in the amyloidogenic fragment of apolipoprotein A-I, J. Biol. Chem. 278 (2003) 2444–2451.
[17] X. Mei, D. Atkinson, Crystal structure of C-terminal truncated apolipoprotein A-I reveals the assembly of HDL by dimerization, J. Biol. Chem. 286 (2011) 38570–38582.
[18] J. Petrlova, T. Duong, M.C. Cochran, A. Axelsson, M. Mörgelin, L.M. Roberts, J.O. Lagerstedt, The fibrillogenic L178H variant of apolipoprotein A-I forms helical fibrils, J. Lipid Res. 53 (2012) 390–398.
[19] J.O. Lagerstedt, G. Cavigiolio, L.M. Roberts, H.S. Hong, L.W. Jin, P.G. Fitzgerald, M.N. Oda, J.C. Voss, Mapping the structural transition in an amyloidogenic apolipoprotein A-I, Biochemistry 46 (2007) 9693–9699.
[20] S.A. Rosú, O.J. Rimoldi, E.D. Prieto, L.M. Curto, J.M. Delfino, N.A. Ramella, M.A. Tricerri, Amyloidogenic propensity of a natural variant of human apolipoprotein a-I: stability and interaction with ligands, PLoS ONE 10 (2015), e0124946.
[21] M. Das, X. Mei, S. Jayaraman, D. Atkinson, O. Gursky, Amyloidogenic mutations in human apolipoprotein A-I are not necessarily destabilizing- a common mechanism of apolipoprotein A-I misfolding in familial amyloidosis and atherosclerosis, FEBS J. 281 (2014) 2525–2542.
[22] O. Gursky, X. Mei, D. Atkinson, The crystal structure of the C-terminal truncated apolipoprotein A-I sheds new light on amyloid formation by the N-terminal fragment, Biochemistry 51 (2012) 10–18.
[23] L. Whitmore, B.A. Wallace, DICHROWEB: an online server for protein secondary structure analyses from circular dichroism spectroscopic data, Nucleic Acids Res. 32 (2004) 668–673.
[24] M. Koyama, M. Tanaka, P. Dhanasekaran, S. Lund-Katz, M.C. Phillips, H. Saito, Interaction between the N- and C-terminal domains modulates the stability and lipid binding of apolipoprotein A-I, Biochemistry 48 (2009) 2529–2537.
[25] B. Hess, C. Kutzner, D. van der Spoel, E. Lindahl, GROMACS 4: algorithms for highly efficient, load-balanced, and scalable molecular simulation, J. Chem. Theory Comput. 4 (2008) 435–447.
[26] S. Pronk, S. Pall, R. Schulz, P. Larsson, P. Bjelkmar, R. Apostolov, M.R. Shirts, J.C. Smith, P.M. Kasson, D. van der Spoel, et al., GROMACS 4.5: a high-throughput and highly parallel open source molecular simulation toolkit, Bioinformatics 29 (2013) 845–854.
[27] D. van der Spoel, R. van Druner, H.J.C. Berendsen, GROningenMAchine for chemical simulations, BIOSON Research Institute, Groningen, The Netherlands, 1994.
[28] H.J.C. Berendsen, J.P.M. Postma, W.F. van Gusteren, A. Di Nola, J.R. Haak, Molecular dynamics with coupling to an external heat bath, J. Chem. Phys. 81 (1984) 3684–3690.
[29] T. Darden, D. York, L. Pedersen, Particle mesh Ewald — an N·log(N) method for Ewald sums in large systems, J. Chem. Phys. 98 (1993) 10089–10092.
[30] G. Bussi, D. Donadio, M. Parrinello, Canonical sampling through velocity rescaling, J. Chem. Phys. 126 (2007) 014101.
[31] M. Parrinello, A. Rahman, Polymorphic transitions in single crystals: a new molecular dynamics method, J. Appl. Phys. 52 (1981) 7182–7190.
[32] B. Hess, H. Bekker, H.J.C. Berendsen, J.G.E.M. Frajie, LINCS: a linear constraint solver for molecular simulations, J. Comput. Chem. 18 (1997) 1463–1472.
[33] A. Merlino, L. Mazzarella, A. Carannante, A. Di Fiore, A. Di Donato, E. Notomista, F. Sica, The importance of dynamic effects on the enzyme activity: X-ray structure and molecular dynamics of onconase mutants, J. Biol. Chem. 280 (2005) 17953–17960.
[34] I. Di Lelio, S. Caccia, M. Coppola, M. Buonanno, G. Di Prisco, P. Varricchio, E. Franzetti, G. Corrado, S.M. Monti, R. Rao, et al., A virulence factor encoded by a polydnavirus confers tolerance to transgenic tobacco plants against lepidopteran larvae, by impairing nutrient absorption, PLoS ONE 9 (2014), e113988.
[35] H. Saito, P. Dhanasekaran, D. Nguyen, P. Holvoet, S. Lund-Katz, M.C. Phillips, Domain structure and lipid interaction in human apolipoproteins A-I and E, a general model, J. Biol. Chem. 278 (2003) 23227–23232.
[36] M. Tanaka, P. Dhanasekaran, D. Nguyen, S. Ohta, S. Lund-Katz, M.C. Phillips, H. Saito, Contributions of the N- and C-terminal helical segments to the lipid-free structure and lipid interaction of apolipoprotein A-I, Biochemistry 45 (2006) 10351–10358.
[37] J.A. Beckstead, B.L. Block, J.K. Bielicki, C.M. Kay, M.N. Oda, R.O. Ryan, Combined N- and C-terminal truncation of human apolipoprotein A-I yields a folded, functional central domain, Biochemistry 44 (2005) 4591–4599.
[38] D.P. Rogers, C.G. Brouillette, J.A. Engler, S.W. Tendian, L. Roberts, V.K. Mishra, G.M. Anantharamaiah, S. Lund-Katz, M.C. Phillips, M.J. Ray, Truncation of the amino terminus of human apolipoprotein A-I substantially alters only the lipid-free conformation, Biochemistry 36 (1997) 288–300.
[39] M. Tanaka, P. Dhanasekaran, D. Nguyen, M. Nickel, Y. Takechi, S. Lund-Katz, M.C. Phillips, H. Saito, Influence of N-terminal helix bundle stability on the lipid-binding properties of human apolipoprotein A-I, Biochim. Biophys. Acta 1811 (2011) 25–30.
[40] V. Granata, G. Graziano, A. Ruggiero, G. Raimo, M. Masullo, P. Arcari, L. Vitagliano, A. Zagari, Chemical denaturation of the elongation factor 1 alpha isolated from the hyperthermophilic archaeon *Sulfolobus solfataricus*, Biochemistry 45 (2006) 719–726.
[41] F. Dal Piaz, A. Casapullo, A. Randazzo, R. Riccio, P. Pucci, G. Marino, L. Gomez-Paloma, Molecular basis of phospholipase A2 inhibition by petrosaspongiolide M, Chembiochem 3 (2002) 664–671.
[42] G. Esposito, R. Michelutti, G. Verdone, P. Viglino, H. Hernàndez, C.V. Robinson, A. Amoresano, F. Dal Piaz, M. Monti, P. Pucci, et al., Removal of the N-terminal hexapeptide from human β2-microglobulin facilitates protein aggregation and fibril formation, Protein Sci. 9 (2000) 831–845.

[43] M. Monti, S. Principe, S. Giorgetti, P. Mangione, G. Merlini, A. Clark, V. Bellotti, A. Amoresano, P. Pucci, Topological investigation of amyloid fibrils obtained from β2-microglobulin, Protein Sci. 11 (2002) 2362–2369.
[44] H. Yagi, K. Hasegawa, Y. Yoshimura, Y. Goto, Acceleration of the depolymerization of amyloid β fibrils by ultrasonication, Biochim. Biophys. Acta 1834 (2013) 2480–2485.
[45] S. Grudzielanek, V. Smirnovas, R. Winter, Solvation-assisted pressure tuning of insulin fibrillation: from novel aggregation pathways to biotechnological applications, J. Mol. Biol. 356 (2006) 497–509.
[46] M. Lindgren, P. Hammarström, Amyloid oligomers: spectroscopic characterization of amyloidogenic protein states, FEBS J. 277 (2010) 1380–1388.